Journal of Chemical Technology & Biotechnology / Volume 96, Issue 8 / p. 2208-2218

Research Article | Full Access

Antimycotic nail polish based on humic acid-coated silver nanoparticles for onychomycosis

Ketheleen N M Dantas, Lucas R Andrade, Erika Lisboa, Victoria L Santana, André L S Santos, Thaís P Mello, Leandro S Sangenito, Álvaro S Lima, Alini T Fricks, Andreza F Begnami, Amanda Cano ... See all authors

First published: 20 January 2021
https://doi-org.lproxy.yeditepe.edu.tr/10.1002/jctb.6676
Citations: 2

Abstract

BACKGROUND

The objective of this work was the development of silver nanoparticles (AgNPs) coated with humic acid (HA) and their incorporation into an enamel for antifungal activity. AgNPs were synthesized by chemical reduction using sodium borohydride as a reducing agent and coated with HA. Uncoated AgNPs were synthesized as control. AgNPs and HA-AgNPs were characterized by ultraviolet–visible spectrophotometry, differential scanning calorimetry, dynamic light scattering, Fourier-transform infrared spectroscopy (FTIR), atomic force microscopy and X-ray diffraction (XRD). Size of AgNPs and HA-AgNPs was recorded within the nano range, showing HA-AgNPs' higher stability than non-coated particles by presenting a single plasmatic band around 400 nm.

RESULTS

Thermal analysis showed conjugated endothermic peaks, which confirms the compatibility of HA-AgNPs. FTIR depicted absorptions between 1300 and 1000 cm^{-1} (C C, Ar—H, respectively), demonstrating that HA is adsorbed onto AgNPs. Thermogravimetric analysis showed that HA does not alter the reduction in mass loss of AgNPs, while it was found by XRD that adding HA promoted the formation of more amorphous AgNPs. The effectiveness of HA-AgNPs was evaluated against three different fungal species. Minimum inhibitory concentration assays showed that ~0.5 mmol L^{-1} AgNPs was able to inhibit dermatophyte species growth. HA-AgNPs were incorporated into a commercial enamel at a concentration of 8% and their organoleptic characteristics, drying time,

centrifugation test and thermal stress were evaluated. Enamels with AgNPs kept their physicochemical properties over 21 days of storage.

CONCLUSION

HA-AgNP nail polish is thus proposed as an innovative material for onychomycosis infections. © 2021 Society of Chemical Industry

INTRODUCTION

Onychomycosis is a pathology that mostly affects the nails,[1] with an incidence rate of around 20% of the adult population worldwide, being more common in men than in women.[2] It is caused by dermatophyte fungi, such as *Trichophyton rubrum* and *T. mentagrophytes*, and yeasts such as *Candida albicans* and *C. parapsilosis*.[3, 4] Contagion usually occurs through direct or indirect contact with contaminated objects, such as sandpaper, pliers and nail clippers. The number of research studies on nail polishes as fomites has grown.[5, 6] Conventional treatment is usually administered orally, and used to be time consuming, causing important side effects.[2] Thus the development of new therapeutic alternatives that provide faster and more effective treatment is in demand.[7, 8] The topical administration route has become a promising treatment option, such as ciclopirox olamine, fluconazole, terbinafine, tioconazole and amorolfine.[9] However, it is recommended as a daily use or three times per week, depending on the active ingredient, with an average treatment duration of 6–12 months.[10]

While nanotechnology is still looking for some alternatives to promote more effective therapies, several types of nanoparticles (NPs) are already used for antifungal applications.[11-15] Among these, silver nanoparticles (AgNPs) are one of the most popular as they show antimicrobial and antifungal activity.[16-19] AgNPs can be obtained from physical, chemical or biological processes. The easiest, most time-saving and most conventional method is a chemical reduction using silver reducing agents such as $NaBH_4$, which has high reactivity and low toxicity.[20-22] In order to create a coat against coalescence phenomena, it is essential to surface-tailor the NPs with a stabilizing agent. In this work, humic acid (HA) was used as a coating agent because of its chelating potential towards metals and metallic ions,[23] and also to avoid the aggregation of NPs.[24, 25] HA (Fig. 1) is a macromolecule composed of humic substances (HS), which are naturally occurring organic compounds. Among the properties of HS, the complexation of metal ions, solubilization, hydrolysis, adsorption and transport are highlighted.[25] This is due to the amphiphilic nature of these substances.[26, 27] The interaction of HA with AgNPs occurs between carboxylate groups and C—O and C—O—C bonds, while HA causes Ag^+ to be reduced to $Ag^{(0)}$.[28, 29] The HA coating of AgNPs can considerably modify the rates of aggregation,[25] dissolution and stability of NPs.[30]

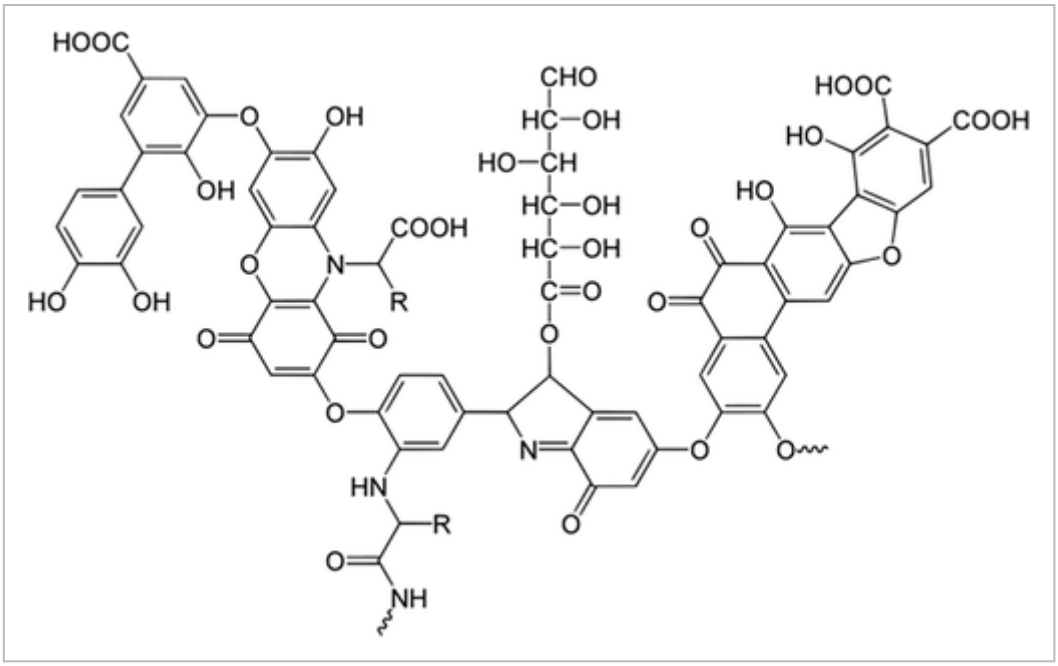

Figure 1

Open in figure viewer | PowerPoint

Chemical structure of humic acid.

The aim of this work was the development of AgNPs coated with HA for use as a raw material for enamels as a preservative of cosmetic formulations. This combination is expected to decrease the risk of contamination and to promote the treatment of onychomycosis infections.

MATERIALS AND METHODS

Materials

HA, $NaBH_4$ and NaOH were purchased in commercial form from Sigma-Aldrich (Darmstadt, Germany). Silver nitrate ($AgNO_3$) was obtained from Dinâmica Química Contemporânea (Indaiatuba, São Paulo, Brazil). Double-distilled water was used in every experiment.

Synthesis of AgNPs

AgNP synthesis was adapted from Dubas and Pimpan.[23] An HA aqueous solution (10 mg L^{-1}) of pH 11.6 was prepared using a magnetic stirrer (K40-1820, Kasvi, Brazil). Then, 10 mL HA, 10 mL $NaBH_4$ (10 mmol L^{-1}) and 3 mL $AgNO_3$ (1 mmol L^{-1}) were homogenized by magnetic stirring (K40-1820, Kasvi) for 30 min at room temperature and without light. The same methodology was repeated in order to produce a control sample (AgNPs without HA).

UV–visible spectroscopy

For the analysis of AgNPs, a Libra S22 UV–visible spectrophotometer (Biochorom, Cambridge, UK) was used with a scanning range from 320 to 470 nm, since AgNPs have

shown intensive and distinct absorption peaks between 380 and 450 nm.[31, 32] Distilled water was used as a reference sample ('blank') and the samples were analyzed at 0 and 90 days since synthesis.[33]

Determination of size, polydispersity index (PDI) and zeta potential (ZP)

The Z-average, PDI and ZP of NPs were determined by photon correlation spectroscopy (PCS; ZetaSizer Nano ZS, Malvern Instruments, Malvern, UK). The analyses were performed at 25 °C, with an He–Ne laser at 633 mW with a wavenumber of 632.8 nm. An aliquot with a dilution factor of 1:100 was taken at half the height of the cuvette and measured in triplicate.[34]

Thermal analysis: differential scanning calorimetry (DSC) and thermogravimetric analysis (TGA)

Thermal analyses were performed using DSC (DSC-60, Shimadzu, Kyoto, Japan) and (TGA; SDTQ600, TA Instruments, Tokyo, Japan). DSC curves were recorded in the range of 0–250 °C, under a nitrogen atmosphere (N_2) with a flow rate of 50 mL min^{-1} and heating rate of 10 °C min^{-1}.[35] TGA curves were recorded on a thermogravimetric instrument, in the range of 30–900 °C, under N_2 with a flow rate of 50 mL min^{-1} and heating rate of 10 °C min^{-1}.[36]

Fourier transform-infrared spectroscopy (FTIR)

FTIR was performed using a spectroscope ATR (total attenuated reflection) device (model Cary 630, Agilent Scientific Instruments, Santa Clara, CA, USA), on a ZnSe spectral scale 4000-400 cm^{-1} and 2 cm^{-1} resolution, and processed for automatic data acquisition in Agilent MicroLab PC software.[37]

X-ray diffraction (XRD)

XRD allowed the evaluation of a crystallinity degree in scanning mode on a Diffractometer (STOE, STADI P, Darmstadt, Germany) operating at a voltage of 30 kV and current of 15 mA, scanning speed of (2θ) = 0.01 min^{-1}, with a time of acquisition of 5 s for each step, and with CuKα radiation (λ = 1.54060 Å).[38]

Atomic force microscopy (AFM)

The morphology of NPs was assessed by AFM. The images were obtained in contact mode with an Easy Scan 2 Basic Instrument AFM (Nanosurf, SC Instruments, Les Ulis, France).[39]

Minimum inhibitory concentration (MIC)

The susceptibility of yeast (*Candida albicans*) and dermatophytes (*Microsporum gypseum*, *M. canis* and *Epidermophyton floccosum*) was carried out according to the microdilution method.

HA, AgNPs and HA-coated AgNPs were evaluated at concentrations of 1, 0.9, 0.8, 0.7, 0.6, 0.5, 0.4, 0.3, 0.2, 0.1 and 0.05 mmol L^{-1} and 5% diluted in RPMI 1640 medium. To each of the wells (96-well plate) 10^2 yeasts or 10^3 dermatophytes were added according to the Institute of Clinical Standards and Laboratories protocol M27-S4 for yeasts and M38-2A for filamentous fungi. The following controls were performed: (i) pure RPMI 1640 medium and (ii) RPMI 1640 medium with fungi without the compounds. Visual reading of the plates was performed after incubation at 37 °C for 48 h for yeasts and 96 h for dermatophytes.

Incorporation AgNPs into nail polish

AgNPs (8%, w/v) were added to commercial nail polish (Risque®) under continuous manual homogenization.[40] The colorless sample (i), light pink: countess (ii), red: coffee bean (iii), and brown (iv) were studied. The nail polish was characterized by drying time applying about 200 µL of nail polish on a disc of artificial nails. The time required for complete drying was observed until it was no longer viscous.[41] All samples were submitted to stability analysis at 5 and 45 °C, for 30 min. After this time, it was observed whether there was either phase separation or changes in its texture. Finally, the centrifugation test was performed in duplicate, using a Daiki centrifuge (digital microprocessor, 16 000 rpm). In this study, 1 mL of each sample was placed in Eppendorf tubes and then subjected to centrifugation, at increasing rotations of 800, 1800 and 3000 rpm, remaining for 15 min at each speed, at room temperature. The formulations were analyzed microscopically in order to check their appearance, phase changes, turbidity and changes in opacity *versus* translucency over the time of the experiment.[42]

RESULTS AND DISCUSSION

The formation of NPs is confirmed when the color of AgNPs changes from light yellow to brown. The chemical reaction describing this change of color is the dissociation of $AgNO_3$ into Ag^+ and NO_3^- ions.[43] The tested formulations consisted of HA-coated AgNPs and uncoated AgNPs (without HA tailoring their surface), both characterizing colloidal systems of yellow color and visually stable for 90 days. According to Mulfinger *et al*.,[44] the yellow color is typical of colloidal silver (Ag^0) due to the absorption of electromagnetic radiation in resonance with surface plasmons. The color of the formulation may vary with particle size: the yellowish color may change to orange and violet, showing that there is an increase in the particle size from the nano to micro scale, and may even develop a silver color if reaching the macroscopic scale.

UV–visible spectroscopy

Figure 2 shows the UV–visible spectroscopy of AgNPs obtained with and without HA coating, measured on day 0 (synthesis) and after 90 days. The formation of a single plasmonic band on the surface of each solution was observed. All samples showed the typical yellow color of the solution,[45] suggesting the formation of AgNPs in both formulations.[46]

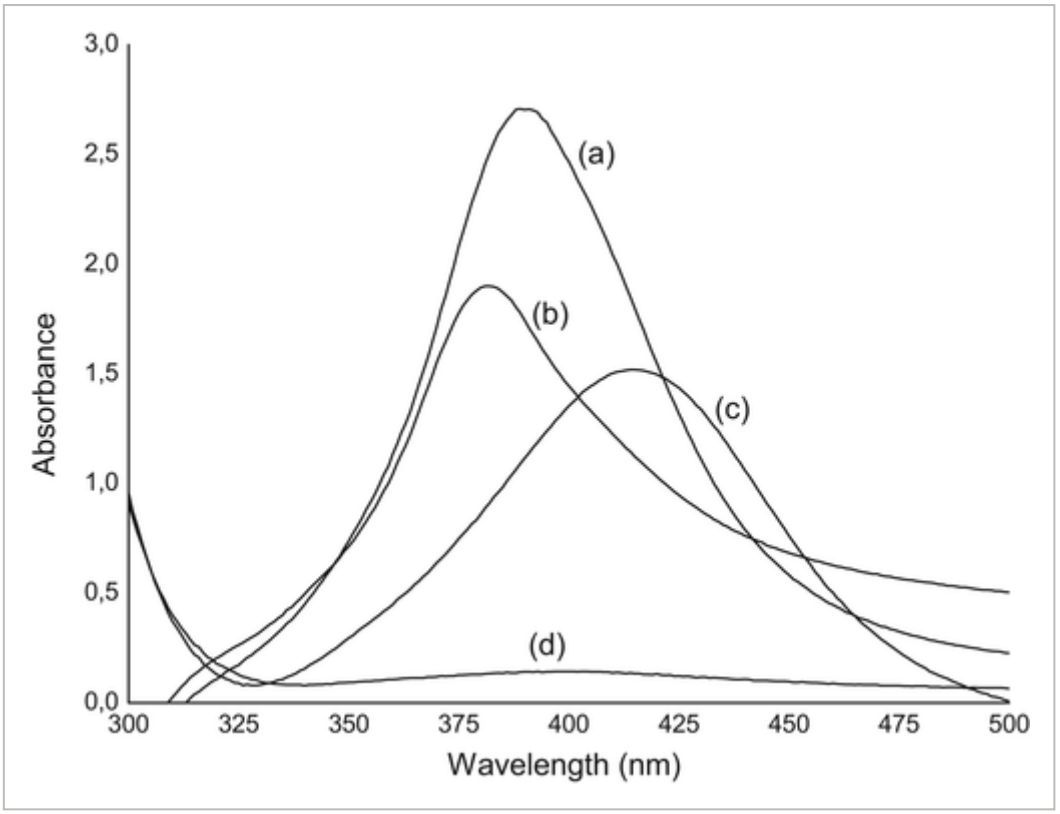

Figure 2

Open in figure viewer | PowerPoint

UV–visible spectra to identify the evolution of the plasmon band as a function of the reduction time of Ag^+ ions according to the frequency of incident light oscillation. (a) AgNPs + HA on day 0; (b) AgNPs on day 0; (c) AgNPs + HA after 90 days; (d) AgNPs after 90 days.

The plasmonic band was noticed after the synthesis, with peaks at about 393 and 385 nm, and was similar to the results reported by Dubas and Pimpan[47] for UV–visible analysis. In our study, the AgNPs were formulated with $NaBH_4$ and coated with HA via chemical synthesis, and the obtained plasmatic bands were around 400 nm. AgNPs stabilized with HA showed a longer wavelength than AgNPs (on day 0), which was attributed to the presence of HA. After 90 days, uncoated AgNP (without HA) did not show a peak in UV–visible absorption, indicating that only $NaBH_4$ was not able to achieve a stable coating onto the particles over time.[48]

AgNPs coated with HA showed a slight displacement of the band to the right with an increase in wavelength from 393 nm to 414 nm, and a reduction in the absorbance peak. This might suggest an increase in particle size due to the coating with HA, which occurred during the synthesis. These data are in agreement with Fernando and Zhou,[49] who synthesized AgNPs using $NaBH_4$ as a reducing agent and added HA in different concentrations (from 0 to 20 mg L^{-1}) to test the stability of AgNPs. In our study, a UV–visible characterization was performed for 14 days in order to observe the changes in the plasmonic bands. Over the period of analysis, uncoated AgNPs showed a gradual decrease

in the peak wavelength, while HA-coated AgNPs exhibited a shift of the band to the right with a slight reduction in peak absorbance.

Determination of Z-average, PDI and ZP

The results of Z-average, PDI and ZP were 92.25 ± 8.4 nm, PDI = 0.69 ± 0.22 and ZP = −3.59 mV ± 0.3 for the uncoated particles (AgNPs) and 78.4 ± 12.7, PDI = 0.31 ± 0.14, ZP = −23.43 mV ± 3.36 for the coated particles (HA-coated AgNP). It has been noticed that the average diameters of NPs obtained by a different methods varied from 50 to 1000 nm, and AgNPs tend to have sizes smaller than 100 nm.[50] In addition, PDI usually corresponds to the particle size within a sample relative to its intensity distribution[51, 52] for which values up to 0.3 indicate a homogeneous distribution.[53] PDI values higher than 0.3 suggest heterogeneity of the sample. In this work, AgNPs coated with HA exhibited homogeneity, which means that most particles had a similar Z-average, being a monodisperse population which ensures uniformity of the physicochemical properties within the sample.

As HA shows an amphiphilic character, these macromolecules may form colloidal species in solution. The Z-average, PDI and ZP obtained for AH isolate were 216.9 ± 34.7 nm, PDI 0.53 ± 0.08 and −34.76 ± 3.13 mV, respectively, which were found to be similar to those reported by de Melo *et al*.,[26] in which the samples coated with HA had a Z-average of 192.41 nm and PDI 0.46, while ZP was about −32.03 mV. These results corroborate the assumption that HA is not self-assembled in solution but is covering the particles.

The ZP reveals the surface charge of the particles and, according to the literature, a value higher than |±30 mV| provides a higher stability for the formulation.[54] AgNPs with and without HA showed values of −23.43 mV ± 3.36 and −3.59 mV ± 0.3, respectively. These data corroborate the data obtained by UV–visible, which showed that the samples coated with HA remained stable for 90 days,[55] while the samples developed only with $NaBH_4$ were not that stable, mainly due to the surface modification of the former.

Thermal analysis

Figure 3 shows the thermogram of $AgNO_3$, HA and AgNPs with and without HA coating. The obtained results are also summarized in Table 1. $AgNO_3$ showed an endothermic peak at 115 °C and ΔH = −889.88 J g^{-1} (onset 80 °C and termination 165 °C) attributed to the fusion,[56] while HA showed an endothermic peak at 118 °C and ΔH = −330.4 J g^{-1} (area of integration between the points of 70 and 182 °C). The HA showed a broad peak due to the heterogeneity of the compound, in which water molecules had weaker interactions with a lower vaporization temperature and stronger interactions with a higher vaporization temperature.[57]

Figure 3

DSC curves of $AgNO_3$, HA, uncoated AgNPs and HA-coated AgNPs.

Table 1. DSC results of humic acid (HA), uncoated silver nanoparticles (AgNPs) and HA-coated AgNPs

Sample	Peak temperature (°C)	Onset temperature (°C)	Termination temperature (°C)	ΔH (J g^{-1})
HA	118.62	70	182	−330.4
$AgNO_3$ peak 1	115	80	165	−889.88
$AgNO_3$ peak 2	209	207	211	−1.84
AgNPs peak 1	61.7	40	65	−93.58
AgNPs peak 2	120	110	145	−79.92
AgNPs + HA peak 1	57.7	46	67	−134.61
AgNPs + HA peak 2	82.08	75	100	−34.70
AgNPs + HA peak 3	126.8	106	175	−209.88

The uncoated AgNPs exhibited two endothermic processes: the first peak with a maximum of 61.7 °C and ΔH = −93.58 J g^{-1} (area of integration obtained between 40 °C and 65 °C), which is typical of the fusion of $AgNO_3$; whereas the second peak appeared with maximum at 120 °C and ΔH = −79.92 J g^{-1} (area of integration obtained between the points 110 and 145 °C). Based on the DSC curves (Fig. 3), the AgNPs showed an endothermic peak at 61.7 °C (ΔH = −93.58 J g^{-1}) and 120 °C (ΔH = −79.92 J g^{-1}). The first peak is characteristic of the fusion of $AgNO_3$, while the second peak may indicate that phytocompounds responsible for the reduction of NPs have low thermal stability, as reported by Sripriya *et al*. (2019).[58]

Similar to uncoated AgNPs, in HA-coated AgNPs it was also possible to observe two endothermic processes and a few peaks between 75 and 100 °C, the highest value being 57.7 °C and ΔH = −134.61 J g^{-1} (area of integration obtained between points 46 and 67 °C). This temperature variation could exist due to the different interactions with the additional components. The peaks between 75 and 100 °C can be attributed to $AgNO_3$ traces of the synthesis that interacted with HA, while the third peak appears at 126.8 °C and ΔH = −209.88 J g^{-1} (area of integration between 106 and 175 °C). The difference in energy involved in this

process is shown for uncoated HA, in which the ΔH of water vaporization is high due to interactions with the several functional groups of the compound, such as the —OH groups.

The presence of two endothermic events in AgNPs is characteristic of these processes, both appearing regardless the presence of HA. The same occurred when AgNPs were coated with polyvinyl alcohol/β-cyclodextrin.[59] AgNPs were characterized by two endothermic peaks, which occurred even when stabilizing agents were added, suggesting that NPs did not suffer any significant change in their thermal stability.

Figure 4 corresponds to the TG curves of the HA, $AgNO_3$ and AgNPs samples with and without HA. Based on TGA analysis of the $AgNO_3$ sample, two stages can be observed, in which the sample decomposes (through the first derivatives). At 364 °C the mass loss of 35.4% of the sample is presented with DTG peaks at 434.8 and 476.7 °C, attributed to the decomposition to NO_2,O_2 and Ag. This is linked to the boiling point of $AgNO_3$, which is 444 °C, thus followed by decomposition.[60] From the analysis of the TG curve of HA, a decrease in the percentage of constant mass, without stabilization steps, was noticed. Degradation of HA starts before 50 °C and is constant. The HA showed a loss of mass of 18.5% between room temperature and 140 °C, with a peak at 53.8 °C. From 100 to 600 °C the mass loss was 51.24%, and up to 900 °C the residual mass was 39.88%.

Figure 4

Open in figure viewer | PowerPoint

TGA (a) and DTG (b) curves of samples of $AgNO_3$, HA, uncoated AgNPs and HA-coated AgNPs.

Analyzing the TG curve of the uncoated AgNPs, the degradation event begins at around 50 °C, attributed to the presence of NO_2, CO_2 and O_2 in the sample, causing mass variation. Then, a relatively constant degradation is observed close to 700 °C, followed by a considerable decrease in the percentage of residual mass attributed to the last traces of silver and residual material.[61-63] The high thermal conductivity of AgNPs explains the low decomposition temperature observed, as demonstrated by Ogundare and van Zyl.[64]

Both HA-coated AgNP and uncoated AgNP curves depict an initial degradation, also given the presence of NO_2, CO_2 and O_2 in these samples. However, it has been noticed that the degradation curve is less pronounced, which can be compared to the TG curve of HA. This constant degradation observed from 300 °C in the first derivative refers to HA up to approximately 500 °C, when the curve begins stabilize. This stabilization refers to the presence of residual silver. The use of HA for the stabilization of AgNPs does not result in large differences in mass loss as a function of temperature. According to Hao *et al*.,[65] the thermal decomposition below 100 °C is related to the evaporation of water still present in

the system. Also, when comparing the TGA results of HA-coated AgNPs with HA alone it is possible to calculate the percentage of silver in the sample.

Infrared absorption spectroscopy (FTIR)

Figure 5 shows the spectrum in the infrared region. The HA sample showed its main functional groups pattern and their respective absorption regions: antisymmetric and symmetric stretch of aliphatic C—H (2920 and 2850 cm^{-1}); from C O and —C—OH groups (1720–1708 cm^{-1}); folding vibrations of the CH_2 and CH_3 groups (1450–1420 cm^{-1}), the widening of the aromatic CH and aliphatic C—OH rings (965 cm^{-1}) and the vibrational planes of the aromatic CH, benzene and alkylbenzene bonds present in the HA molecule (829 cm^{-1}).[66-68] The sample of $AgNO_3$ showed two absorption bands in the infrared region of the asymmetric stretching of the nitrate ion (NO^{3-}) that can be observed in the region of weak signal stretching (1772–1751 cm^{-1}) and of the strong signal band in the region (1270 cm^{-1}). Moreover, a similarity between the FTIR results of $AgNO_3$ and AgNPs can also be seen. Both samples exhibited major bands of intensity similar to the existing bands in the spectrum corresponding to the region between 3500 and 3000 cm^{-1}, which may be due to the presence of water in the analyzed samples. In both cases, peaks around 1384 cm^{-1} were observed, which is characteristic of N—O and N O stretching of NO_3. Therefore, these bands are attributed to the NO^{3-} residual of the $AgNO_3$ solution.[69, 70]

Figure 5

Open in figure viewer | PowerPoint

FTIR spectra of HA, $AgNO_3$, uncoated AgNPs and HA-coated AgNPs.

According to the literature, the bands around 2920, 2852, 1640 and 1500 cm^{-1} are reported to be typical of AgNPs, showing a similar FTIR pattern, as reported by Wang *et al*.[68] and Behboudi *et al*.[71]

Similarly, Hao *et al*.[65] synthesized AgNPs assisted by HA and compared HA spectra with those of AgNPs. The OH and C O elongation absorption peaks showed a slight change, as shown in our results. This suggests that HA interacts with AgNPs by carboxyls and phenolic hydroxyls groups, thus being adsorbed onto the surface of NPs.

Atomic force microscopy (AFM)

The morphology of the AgNP samples with and without HA was investigated by AFM (Fig. 6). The synthesized NPs were mostly spherical. HA-coated AgNPs had a mean size of around 121 nm, while uncoated AgNPs were of about 130 nm. These results are in agreement with those reported by Pereira *et al*.,[72] who synthesized AgNPs with a Z-average of 138.8 nm, and where the HA-coated AgNPs were slightly smaller than the uncoated AgNPs.

Figure 6

Open in figure viewer | PowerPoint

AFM image of uncoated AgNPs (a) and of HA-coated AgNPs (b).

Figure 7 shows the size distribution of HA-coated AgNPs, in which a slight variation in the sizes can be seen, corroborating the results obtained by PCS analysis.

Figure 7

Open in figure viewer | PowerPoint

Particle size distribution of HA-coated AgNPs based on AFM analysis.

X-ray diffraction

XRD helps in the characterization of the crystalline and polymorphic structure of materials. Diffractograms of $AgNO_3$, HA, HA-coated AgNPs and uncoated AgNPs are shown in Fig. 8. Based on HA diffractograms, it is possible to observe that the sample was semi-amorphous (unordered peaks). Although this sample did not represent any defined shape, some areas were well defined by crystallinity peaks.

Figure 8

Open in figure viewer | PowerPoint

Diffractograms of $AgNO_3$, HA, uncoated AgNPs and HA-coated AgNPs.

XRD bands of $AgNO_3$ showed a large diffraction profile characterized by high-intensity peaks. The sample had a single phase: 43.615°, 62.328° and 80.472°. The phases have a relation with the Ag phase present in $AgNO_3$. The same peaks were identified by Htwe *et al*. (2019),[73] which correspond to the planes of the crystalline cubic structure of Ag.

Moreover, AgNP diffractograms exhibited a crystalline structure with peaks of intensity at different angles. Peaks were identified at 15°, 17°, 20°, 30° and 38°, the latter being the characteristic Ag peak which corresponds to the plane in a cubic structure with a centered face of Ag. Thus it is a characteristic peak of AgNPs, which was already identified by Dayakar *et al*.[74] and Ravichandran *et al*.[75]

Finally, diffractograms of HA-coated AgNPs showed peaks with a lower intensity than those of AgNPs (without HA coating). Peaks referring to the $AgNO_3$ diffractogram also appeared in

the diffractogram of HA-coated AgNPs with similar intensities, especially the peak at 38°, identified for Ag. All these features suggest that the use of HA as a stabilizing agent of AgNPs might cause a change in their crystallinity, creating a more amorphous structure.[76-79]

MIC assay

The antimicrobial and antifungal activity of AgNPs has been already widely described in the literature.[80-83] However, HA-coated AgNPs are a new formulation for these purposes. Table 2 shows the results of the MIC assay of the uncoated AgNPs and AH-coated AgNPs.

Table 2. Results of MIC assay obtained for uncoated silver nanoparticles (AgNPs) and humic acid (HA)-coated AgNPs

Gender/species	Uncoated AgNPs (mmol L^{-1})	HA-coated AgNPs (mmol L^{-1})
Candida albicans	0.4	0.7
Microsporum canis	0.9	0.8
Microsporum gypseum	1.0	1.0
Epidermophyton floccosum	0.6	0.5

The results showed an improved activity of HA-coated AgNPs compared with uncoated AgNPs, with the exception of those tested in the yeast *Candida albicans*, which inhibited growth with a lower concentration compared to HA-coated AgNPs. Uncoated AgNPs promoted inhibition with a concentration of 0.4 mmol L^{-1} $AgNO_3$ (40%), whereas HA-coated AgNPs resulted in concentrations of 0.7 mmol L^{-1} $AgNO_3$. This fact has not been previously described in the literature, and may suggest that the uncoated AgNPs release metal ions more quickly than the coated, thus increasing the risk of cell toxicity.

Fernando and Zhou[49] reported that HA acts by reducing the release of Ag ions. This fact may justify the hypothesis that AgNPs have a better action with the analyzed species, probably due to the rapid release of these ions causing toxicity. In the analysis with dermatophyte genera, an inhibition of 0.0 mmol L^{-1} with uncoated AgNPs (corresponding to 0.9 mmol L^{-1} $AgNO_3$) was obtained, whereas with HA-coated AgNPs the inhibition seen with 0.8 mmol L^{-1} $AgNO_3$ when tested for *M. canis*.

For *M. floccosum* species, the uncoated AgNPs showed a better result with the inhibition activity at 0.6 mmol L^{-1} $AgNO_3$, while with HA-coated AgNPs the inhibition activity was recorded at 0.5 mmol L^{-1} $AgNO_3$. For *M. gypseum*, the inhibition activity was seen only when testing the initial concentrations, regardless of the presence of HA coating.

Enamel characterizations

Enamels composed of 8% HA-coated AgNPs were subjected to analysis using a conventional enamel as control. Drying time and thermal stress tests were carried out at zero time after adding the NPs. Results are detailed in Table 3.

Table 3. Sample drying time and modifications after thermal stress

Color	Sample	Drying time	Modifications after thermal stress [45 °C]	Modifications after thermal stress [5 °C]
Colorless	Control 1	3 min 48 s	N	N
Colorless	Sample 1	3 min 33 s	N	N
Light pink	Control 2	3 min 0 s	N	LM
Light pink	Sample 2	2 min 48 s	LM	LM
Coffee bean	Control 3	4 min 0 s	N	LM
Coffee bean	Sample 3	3 min 0 s	LM	LM
Brown	Control 4	4 min 0 s	N	SF
Brown	Sample 4	3 min 30 s	N	LM

Pure enamel was set as the control and evaluated samples as enamels with the addition of humic acid-coated silver nanoparticles.

Abbreviations: N, unchanged and homogeneous; LM, slightly modified, but without phase separation; SF, not homogeneous, with phase separation.

Once the drying time was verified, a shorter drying time in all of the tested samples containing NPs ('Sample') was seen than in all of samples without NPs ('Control'). After the thermal stress was performed, it was noticed that Samples 2 and 3 became more viscous at

45 °C, while Control 4 and the other samples showed phase separation at 5 °C. For Control 1 and Sample 1, a slight change in consistency without changing homogeneity was noticed.

In the centrifugation test, Samples 2 and 3 exhibited changes at 800 rpm, showing a high viscosity, while the other samples and controls showed no changes. At a centrifugation of 3000 rpm, Control 4 precipitated with a subtle phase separation, whereas all samples including controls were more viscous.

Regarding organoleptic characteristics, the samples with NPs and control samples were tested at zero time, 24 and 72 h, 7 and 21 days after adding the HA-coated AgNPs. The organoleptic characteristics of all controls remained unchanged over the days of the analysis. However, in the case of the enamels with HA-coated AgNPs, Sample 1 instantly turned more opaque when NPs were added, whereas Samples 2–4 became more opaque at 72 h, with an increase in loss of brightness after the observation days, as shown in Fig. 9.

Figure 9

(a) Digital photos of control enamel bottles and enamel with the addition of HA-coated AgNPs at zero time; (b) digital photos of artificial nails showing organoleptic characteristics of the control enamels and samples on different days, being: A, time 0; B, 24 h; C, 72 h; D, 7 days; E, 21 days.

CONCLUSIONS

Because of the cellular similarity between the fungal pathogen and human cells – both eukaryotic organisms – the pharmacotherapy of fungal infections is a challenging task. It is rare to find a substance that has selective toxicity only for the fungus and not causing harm to the patient. The discovery of new molecules that prevent and treat onychomycosis is still incipient. Given this, the development of new nanotechnological strategies for site-specific delivery of active ingredients is receiving much attention. One of the main requirements is the identification of relevant cellular targets to test these therapies. In this scenario new studies in the field of nanotechnology seek alternatives to improve the transungual permeation of assets, decrease treatment time and improve treatment adherence. In the present study, AgNPs with and without HA have been synthesized successfully. All NPs showed spherical morphology with a size of around 100 nm. The HA coating improved the stability of AgNPs, and their incorporation in the nail polish did not influence their physical properties. HA-coated AgNP nail polish is anticipated to be a suitable, innovative and effective alternative for the treatment of onychomycosis.

ACKNOWLEDGEMENTS

This research was financed by the Coordenação Aperfeiçoamento de Pessoal de Nivel Superior (CAPES), Fundação de Amparo à Pesquisa do Estado de Sergipe (FAPITEC) and Conselho Nacional de Desenvolvimento Científico e Tecnológico (CNPq). EBS wishes to acknowledge the sponsorship of the project UIDB/04469/2020 (strategic fund) from the Portuguese Science and Technology Foundation, Ministry of Science and Education (FCT/MEC) through national funds, co-financed by FEDER, under Partnership Agreement PT2020.

CONFLICT OF INTEREST

The authors declare no conflicts of interest.

REFERENCES

1 Zaias N, Escovar S, Zaiac M, Edwards R, Dutra M, Pona A *et al*., Onychomycosis, the active invasion of a normal nail unit by a dermatophytic versus the colonization of an existing abnormal nail unit by environmental fungus. *Skinmed* **18**: 18– 22 (2020).
PubMed | Google Scholar

2 Fávero Maria L. D., Bonetti Aline F., Domingos Eric L., Tonin Fernanda S., Pontarolo Roberto. Oral antifungal therapies for toenail onychomycosis: a systematic review with network meta-analysis toenail mycosis: network meta-analysis. *Journal of Dermatological Treatment*. 2020; 1– 10. http://dx.doi.org.lproxy.yeditepe.edu.tr/10.1080/09546634.2020.1729336 .
Crossref | PubMed | Web of Science® | Google Scholar

3 Lindsø Andersen P, Henning MAS, Jemec GBE, Arendrup MC and Saunte DM, Two cases of proximal subungual onychomycosis caused by *Trichophyton rubrum* in HIV negative patients during treatment with TNF-α inhibitors combined with methotrexate. *Acta Dermatovenerol Croat* **26**: 304– 304 (2018).
PubMed | Web of Science® | Google Scholar

4 Haghani I, Shams-Ghahfarokhi M, Dalimi Asl A, Shokohi T and Hedayati MT, Molecular identification and antifungal susceptibility of clinical fungal isolates from onychomycosis (uncommon and emerging species). *Mycoses* **62**: 128– 143 (2019).
Wiley Online Library | CAS | PubMed | Web of Science® | Google Scholar

5 Klafke GB, Silva RA d, Pellegrin KTD and Xavier MO, Analysis of the role of nail polish in the transmission of onychomycosis. *An Bras Dermatol* **93**: 930– 931 (2018).
Crossref | PubMed | Web of Science® | Google Scholar

6 Reinecke JK and Hinshaw MA, Nail health in women. *Int J Women's Dermatol* **6**: 73– 79 (2020).
Crossref | PubMed | Google Scholar

7 Kerai LV, Bardés J, Hilton S and Murdan S, Two strategies to enhance ungual drug permeation from UV-cured films: incomplete polymerisation to increase drug release and incorporation of chemical enhancers. *Eur J Pharm Sci* **123**: 217– 227 (2018).
Crossref | CAS | PubMed | Web of Science® | Google Scholar

8 Wang X, Fan W, Dong Z, Liang D and Zhou T, Interactions of natural organic matter on the surface of PVP-capped silver nanoparticle under different aqueous environment. *Water Res* **138**: 224– 233 (2018).
Crossref | CAS | PubMed | Web of Science® | Google Scholar

9 M. Mizutani, T. Tanaka, H. Ogino, M. Akazawa, Therapeutic agent for onychomycosis, US Patent Application 16/469,863, 2020.
Google Scholar

10 Ghannoum M and Isham N, Fungal nail infections (onychomycosis): a never-ending story? *PLoS Pathog* **10**: e1004105 (2014).
Crossref | CAS | PubMed | Web of Science® | Google Scholar

11 Carbone C, Fuochi V, Zielińska A, Musumeci T, Souto E, Bonaccorso A *et al*., Dual-drugs delivery in solid lipid nanoparticles for the treatment of *Candida albicans* mycosis. *Colloids Surf B Biointerfaces* **186**: 110705 (2020).
Crossref | CAS | PubMed | Web of Science® | Google Scholar

12 Khatua A, Priyadarshini E, Rajamani P, Patel A, Kumar J, Naik A *et al*., Phytosynthesis, characterization and fungicidal potential of emerging gold nanoparticles using *Pongamia pinnata* leave extract: a novel approach in nanoparticle synthesis. *J Clust Sci* **31**: 125– 131 (2020).
Crossref | CAS | Web of Science® | Google Scholar

13 Elegbede JA, Lateef A, Azeez MA, Asafa T, Yekeen TA, Oladipo I *et al*., Biofabrication of gold nanoparticles using xylanases through valorization of corncob by *Aspergillus niger* and *Trichoderma longibrachiatum*: antimicrobial, antioxidant, anticoagulant and thrombolytic activities. *Waste Biomass Valorization* **11**: 781– 791 (2020).
Crossref | CAS | Web of Science® | Google Scholar

14 El-Batal AI, El-Sayyad GS, Mosallam FM and Fathy RM, *Penicillium chrysogenum*-mediated mycogenic synthesis of copper oxide nanoparticles using gamma rays for in vitro antimicrobial activity against some plant pathogens. *J Clust Sci* **31**: 79– 90 (2020).
Crossref | CAS | Web of Science® | Google Scholar

15 Arshad M, Ehtisham-ul-Haque S, Bilal M, Ahmad N, Ahmad A, Abbas M *et al*., Synthesis and characterization of Zn doped WO_3 nanoparticles: photocatalytic, antifungal and antibacterial activities evaluation. *Mater Res Express* **7**:015407 (2020).
Crossref | CAS | Web of Science® | Google Scholar

16 Sánchez-López E, Gomes D, Esteruelas G, Bonilla L, Lopez-Machado AL, Galindo R *et al*., Metal-based nanoparticles as antimicrobial agents: an overview. *Nanomaterials* **10**: 292 (2020).
Crossref | CAS | Web of Science® | Google Scholar

17 Hissae Yassue-Cordeiro P, Zandonai CH, Pereira Genesi B, Santos Lopes P, Sanchez-Lopez E, Garcia ML *et al*., Development of chitosan/silver sulfadiazine/zeolite composite films for wound dressing. *Pharmaceutics* **11**: 535 (2019).
Crossref | Web of Science® | Google Scholar

18 Diniz FR, Maia RCAP, Rannier L, Andrade LN, Chaud MV, da Silva CF *et al*., Silver nanoparticles-composing alginate/gelatin hydrogel improves wound healing in vivo. *Nanomaterials* **10**: 390 (2020).
Crossref | CAS | Web of Science® | Google Scholar

19 Barbosa GP, Debone HS, Severino P, Souto EB and da Silva CF, Design and characterization of chitosan/zeolite composite films: effect of zeolite type and zeolite dose on the film properties. *Mater Sci Eng C* **60**: 246– 254 (2016).
Crossref | CAS | PubMed | Web of Science® | Google Scholar

20 Ottoni CA, Simões MF, Fernandes S, Dos Santos JG, Da Silva ES, de Souza RFB *et al*., Screening of filamentous fungi for antimicrobial silver nanoparticles synthesis. *AMB Express* **7**: 1– 10 (2017).
Crossref | CAS | PubMed | Web of Science® | Google Scholar

21 Chumpol J and Siri S, Light-mediated green synthesis of DNA-capped silver nanoparticles and their antibacterial activity. *J Nanosci Nanotechnol* **20**: 1678– 1684 (2020).
Crossref | CAS | PubMed | Web of Science® | Google Scholar

22 Murali KI, Bhagavanth RG, Veerabhadram G, Madhusudhan A, Eco-friendly green synthesis of silver nanoparticles using salmalia malabarica: synthesis, characterization, antimicrobial, and catalytic activity studies. *Applied Nanoscience* **5**: 681– 689 (2020).
http://dx.doi.org.lproxy.yeditepe.edu.tr/10.1007/s13204-015-0479-6 .
PubMed | Web of Science® | Google Scholar

23 Dubas ST and Pimpan V, Humic acid assisted synthesis of silver nanoparticles and its application to herbicide detection. *Mater Lett* **62**: 2661– 2663 (2008).
Crossref | CAS | Web of Science® | Google Scholar

24 Lopez ECR, Zafra MA, Gavan JNL, Villena EDA, Almaquer FEP, Perez JVD, Humic Acid Functionalized - Silver Nanoparticles as Nanosensor for Colorimetric Detection of Copper (II) Ions in Aqueous Solutions. *Key Engineering Materials*. 2020; **831**: 142– 150.
http://dx.doi.org.lproxy.yeditepe.edu.tr/10.4028/www.scientific.net/kem.831.142 .
Crossref | Google Scholar

25 Wei Y, Wu X, Zeng R, Cai C and Guo Z, Spatial variations of aggregate-associated humic substance in heavy-textured soils along a climatic gradient. *Soil Tillage Res* **197**: 104497 (2020).

Crossref | Web of Science® | Google Scholar

26 de Melo BAG, Motta FL and Santana MH, Humic acids: structural properties and multiple functionalities for novel technological developments. *Mater Sci Eng C* **62**: 967– 974 (2016).
Crossref | PubMed | Web of Science® | Google Scholar

27 Motta F, Melo B and Santana M, Deprotonation and protonation of humic acids as a strategy for the technological development of pH-responsive nanoparticles with fungicidal potential. *New Biotechnol* **33**: 773– 780 (2016).
Crossref | CAS | PubMed | Web of Science® | Google Scholar

28 Nakamoto K, *Infrared and Raman Spectra of Inorganic and Coordination Compounds, In Handbook of Vibrational Spectroscopy (eds J.M. Chalmers and P.R. Griffiths)*. Wiley, Chichester, UK (2006).
Google Scholar

29 Ding Y, Bai X, Ye Z, Gong D, Cao J and Hua Z, Humic acid regulation of the environmental behavior and phytotoxicity of silver nanoparticles to *Lemna minor*. *Environ Sci Nano* **6**: 3712– 3722 (2019).
Crossref | CAS | Web of Science® | Google Scholar

30 Gunsolus IL, Mousavi MP, Hussein K, Bühlmann P and Haynes CL, Effects of humic and fulvic acids on silver nanoparticle stability, dissolution, and toxicity. *Environ Sci Technol* **49**: 8078– 8086 (2015).
Crossref | CAS | PubMed | Web of Science® | Google Scholar

31 Mohaghegh S, Osouli-Bostanabad K, Nazemiyeh H, Javadzadeh Y, Parvizpur A, Barzegar-Jalali M *et al*., A comparative study of eco-friendly silver nanoparticles synthesis using *Prunus domestica* plum extract and sodium citrate reducing agents. *Adv Powder Technol* **31**: 1169– 1180 (2020).
Crossref | CAS | Web of Science® | Google Scholar

32 M. Skiba, V. Vorobyova, O. Pivovarov, K. Sorochkina, A. Shakun, Plasma-chemical-assisted Voprosy khimii i khimicheskoi tekhnologii, **1**: 53– 60 (2020),
https://doi-org.lproxy.yeditepe.edu.tr/10.32434/0321-4095-2020-128-1-53-60 (2020).
Google Scholar

33 de Melo BAG, Motta FL and Santana MHA, The interactions between humic acids and Pluronic F127 produce nanoparticles useful for pharmaceutical applications. *J Nanopart Res* **17**: 400 (2015).
Crossref | Web of Science® | Google Scholar

34 Andrade LN, Oliveira DM, Chaud MV, Alves TF, Nery M, da Silva CF *et al*., Praziquantel–solid lipid nanoparticles produced by supercritical carbon dioxide extraction: physicochemical characterization, release profile, and cytotoxicity. *Molecules* **24**: 3881 (2019).
Crossref | CAS | Web of Science® | Google Scholar

35 Köroğlu A, Şahİn O, Kürkçüoğlu I, Dede DÖ, Özdemİr T and Hazer B, Silver nanoparticle incorporation effect on mechanical and thermal properties of denture base acrylic resins. *J Appl Oral Sci* **24**: 590– 596 (2016).
Crossref | PubMed | Web of Science® | Google Scholar

36 Amjadi M, Shokri R and Hallaj T, Interaction of glucose-derived carbon quantum dots with silver and gold nanoparticles and its application for the fluorescence detection of 6-thioguanine. *Luminescence* **32**: 292– 297 (2017).
Wiley Online Library | CAS | PubMed | Web of Science® | Google Scholar

37 Ahmed S, Saifullah MA, Swami BL and Ikram S, Green synthesis of silver nanoparticles using *Azadirachta indica* aqueous leaf extract. *J Radiat Res Appl Sci* **9**: 1– 7 (2016).
Crossref | CAS | Web of Science® | Google Scholar

38 Pérez AN, Ojeda M. M, Renteria T VM, Ojeda ML, Velasquez O C. Graphene oxide with the addition of different values of Ag nanoparticles.. *Journal of Physics: Conference Series*. 2019; **1221**: 012013http://dx.doi.org.lproxy.yeditepe.edu.tr/10.1088/1742-6596/1221/1/012013 .
Crossref | CAS | Google Scholar

39 Ali W, Shabani V, Linke M, Sayin S, Gebert B, Altinpinar S *et al*., Electrical conductivity of silver nanoparticle doped carbon nanofibres measured by CS-AFM. *RSC Adv* **9**: 4553– 4562 (2019).
Crossref | CAS | Web of Science® | Google Scholar

40 Cutrín-Gómez E, Anguiano-Igea S, Delgado-Charro MB, Gómez-Amoza JL and Otero-Espinar FJ, Effect on nail structure and transungual permeability of the ethanol and poloxamer ratio from cyclodextrin-soluble polypseudorotaxanes based nail lacquer. *Pharmaceutics* **10**: 156 (2018).
Crossref | CAS | Web of Science® | Google Scholar

41 Cutrín-Gómez E, Anguiano-Igea S, Delgado-Charro MB, Gómez-Amoza JL and Otero-Espinar FJ, Effect of penetration enhancers on drug nail permeability from cyclodextrin/poloxamer-soluble polypseudorotaxane-based nail lacquers. *Pharmaceutics* **10**: 273 (2018).
Crossref | CAS | Web of Science® | Google Scholar

42 ANVISA, Agência Nacional de Vigilância Sanitária, Gerência Geral de cosméticos, Brasilia. (2020). Available: http://portal.anvisa.gov.br/cosmeticos [23 March 2020].
Google Scholar

43 Shuaib U, Hussain T, Ahmad R, Zakaullah M, Mubarik FE, Muntaha ST, Ashraf S, Plasma-liquid synthesis of silver nanoparticles and their antibacterial and antifungal applications. *Materials Research Express*. 2020; **7**: 3: 035015
http://dx.doi.org.lproxy.yeditepe.edu.tr/10.1088/2053-1591/ab7cb6 .
Crossref | CAS | Web of Science® | Google Scholar

44 Mulfinger L, Solomon SD, Bahadory M, Jeyarajasingam AV, Rutkowsky SA and Boritz C, Synthesis and study of silver nanoparticles. *J Chem Educ* **84**: 322 (2007).

Crossref | Web of Science® | Google Scholar

45 Vo T-T, Dang C-H, Doan V-D, Dang V-S and Nguyen T-D, Biogenic synthesis of silver and gold nanoparticles from *Lactuca indica* leaf extract and their application in catalytic degradation of toxic compounds. *J Inorg Organomet Polym Mater* **30**: 388– 399 (2020).
Crossref | CAS | Web of Science® | Google Scholar

46 Freire NB, Pires LC, Oliveira HP and Costa MM, Antimicrobial and antibiofilm activity of silver nanoparticles against *Aeromonas* spp. isolated from aquatic organisms. *Pesqui Vet Bras* **38**: 244–249 (2018).
Crossref | Web of Science® | Google Scholar

47 Dubas ST and Pimpan V, Green synthesis of silver nanoparticles for ammonia sensing. *Talanta* **76**: 29– 33 (2008).
Crossref | CAS | PubMed | Web of Science® | Google Scholar

48 Hoang V-T, Mai M, Thi Tam L, Vu NP, Tien Khi N, Dinh Tam P, Quang Huy T, Le A-T, Xuan Dinh N, Tran V-H, Functionalized-AgNPs for Long-Term Stability and Its Applicability in the Detection of Manganese Ions. *Advances in Polymer Technology*. 2020; Article ID 9437108.
https://doi-org.lproxy.yeditepe.edu.tr/10.1155/2020/9437108 .
Google Scholar

49 Fernando I and Zhou YC, Impact of pH on the stability, dissolution and aggregation kinetics of silver nanoparticles. *Chemosphere* **216**: 297– 305 (2019).
Crossref | CAS | PubMed | Web of Science® | Google Scholar

50 GhavamiNejad A, Rajan Unnithan A, Sasikala ARK, Samarikhalaj M, Thomas RG, Jeong YY *et al*., Mussel-inspired electrospun nanofibers functionalized with size-controlled silver nanoparticles for wound dressing application. *ACS Appl Mater Interfaces* **7**: 12176– 12183 (2015).
Crossref | CAS | PubMed | Web of Science® | Google Scholar

51 Zielinska A, Martins-Gomes C, Ferreira NR, Silva AM, Nowak I and Souto EB, Anti-inflammatory and anti-cancer activity of citral: optimization of citral-loaded solid lipid nanoparticles (SLN) using experimental factorial design and LUMiSizer®. *Int J Pharm* **553**: 428– 440 (2018).
Crossref | CAS | PubMed | Web of Science® | Google Scholar

52 Zielińska A, Ferreira NR, Durazzo A, Lucarini M, Cicero N, Mamouni SE, Silva AM, Nowak Izabela, Santini Antonello, Souto Eliana B.. Development and Optimization of Alpha-Pinene-Loaded Solid Lipid Nanoparticles (SLN) Using Experimental Factorial Design and Dispersion Analysis. *Molecules*. 2019; **24**: 15: 2683.
http://dx.doi.org.lproxy.yeditepe.edu.tr/10.3390/molecules24152683 .
Crossref | CAS | Web of Science® | Google Scholar

53 Souto EB, Doktorovova S, Zielinska A and Silva AM, Key production parameters for the development of solid lipid nanoparticles by high shear homogenization. *Pharm Dev Technol* **24**: 1181– 1185 (2019).

Crossref | CAS | PubMed | Web of Science® | Google Scholar

54 Smith MC, Crist RM, Clogston JD and McNeil SE, Zeta potential: a case study of cationic, anionic, and neutral liposomes. *Anal Bioanal Chem* **409**: 5779– 5787 (2017).
Crossref | CAS | PubMed | Web of Science® | Google Scholar

55 Anandalakshmi K, Venugobal J and Ramasamy V, Characterization of silver nanoparticles by green synthesis method using *Pedalium murex* leaf extract and their antibacterial activity. *Appl Nanosci* **6**: 399– 408 (2016).
Crossref | CAS | Web of Science® | Google Scholar

56 Valle PS, Montesso M, Nalin M, Donoso JP, Silva IDA and Magon CJ, Influência dos precursores de prata no crescimento de nanopartículas metálicas em vidros óxidos de metais pesados. *J Quím Nova* **36**: 967– 971 (2013).
Crossref | CAS | Web of Science® | Google Scholar

57 Sirousazar M and Khodamoradi P, Freeze-thawed humic acid/polyvinyl alcohol supramolecular hydrogels. *Mater Today Commun* **22**: 100719 (2020).
Crossref | CAS | Web of Science® | Google Scholar

58 Sripriya N, Vasantharaj S, Mani U, Shanmugavel M, Jayasree R and Gnanamani A, Encapsulated enhanced silver nanoparticles biosynthesis by modified new route for nano-biocatalytic activity. *Biocatal Agric Biotechnol* **18**: 101045 (2019).
Crossref | Web of Science® | Google Scholar

59 Balakrishnan SB and Thambusamy S, Preparation of silver nanoparticles and riboflavin embedded electrospun polymer nanofibrous scaffolds for in vivo wound dressing application. *Process Biochem* **88**: 148– 158 (2020).
Crossref | CAS | Web of Science® | Google Scholar

60 Janković B, Stopić S, Bogović J and Friedrich B, Kinetic and thermodynamic investigations of non-isothermal decomposition process of a commercial silver nitrate in an argon atmosphere used as the precursors for ultrasonic spray pyrolysis (USP): the mechanistic approach. *Chem Eng Process Intensif* **82**: 71– 87 (2014).
Crossref | CAS | Web of Science® | Google Scholar

61 Butola B and Verma D, Facile synthesis of chitosan-silver nanoparticles onto linen for antibacterial activity and free-radical scavenging textiles. *Int J Biol Macromol* **133**: 1134– 1141 (2019).
Crossref | PubMed | Web of Science® | Google Scholar

62 Maharjan S, Liao K-S, Wang AJ, Zhu Z, McElhenny BP, Bao J *et al*., Sol–gel synthesis of stabilized silver nanoparticles in an organosiloxane matrix and its optical nonlinearity. *Chem Phys* **532**: 110610 (2020).
Crossref | CAS | Web of Science® | Google Scholar

63 Majeed S, Bakhtiar NFB, Danish M, Ibrahim MM and Hashim R, Green approach for the biosynthesis of silver nanoparticles and its antibacterial and antitumor effect against osteoblast MG-63 and breast MCF-7 cancer cell lines. *Sustain Chem Pharm* **12**: 100138 (2019).
Crossref | Web of Science® | Google Scholar

64 Ogundare SA and van Zyl WE, Nanocrystalline cellulose as reducing-and stabilizing agent in the synthesis of silver nanoparticles: application as a surface-enhanced Raman scattering (SERS) substrate. *Surf Interfaces* **13**: 1– 10 (2018).
Crossref | CAS | Web of Science® | Google Scholar

65 Hao Y, Peng J, Hu S, Li J and Zhai M, Thermal decomposition of allyl-imidazolium-based ionic liquid studied by TGA–MS analysis and DFT calculations. *Thermochim Acta* **501**: 78– 83 (2010).
Crossref | CAS | Web of Science® | Google Scholar

66 Dick D, Santos J and Ferranti E, Chemical characterization and infrared spectroscopy of soil organic matter from two southern Brazilian soils. *Rev Bras Ciênc Solo* **27**: 29– 39 (2003).
Crossref | CAS | Web of Science® | Google Scholar

67 Zhang L, Zeng G, Dong H, Chen Y, Zhang J, Yan M *et al*., The impact of silver nanoparticles on the co-composting of sewage sludge and agricultural waste: evolutions of organic matter and nitrogen. *Bioresour Technol* **230**: 132– 139 (2017).
Crossref | CAS | PubMed | Web of Science® | Google Scholar

68 Wang L, Wu Y, Xie J, Wu S and Wu Z, Characterization, antioxidant and antimicrobial activities of green synthesized silver nanoparticles from *Psidium guajava* L. leaf aqueous extracts. *Mater Sci Eng C* **86**: 1– 8 (2018).
Crossref | PubMed | Web of Science® | Google Scholar

69 Sameen A, Fathima SJ, Ramlal S, Kumar S and Khanum F, Nanopackaging of silver using spice extract and their characterization. *Sci Technol Arts Res J* **3**: 52– 56 (2014).
Crossref | CAS | Google Scholar

70 Balavandy SK, Shameli K, Biak DRBA and Abidin ZZ, Stirring time effect of silver nanoparticles prepared in glutathione mediated by green method. *Chem Cent J* **8**: 11 (2014).
Crossref | PubMed | Google Scholar

71 Behboudi A, Jafarzadeh Y and Yegani R, Enhancement of antifouling and antibacterial properties of PVC hollow fiber ultrafiltration membranes using pristine and modified silver nanoparticles. *J Environ Chem Eng* **6**: 1764– 1773 (2018).
Crossref | CAS | Web of Science® | Google Scholar

72 Pereira AGB, Martins AF, Paulino AT, Fajardo AR, Guilherme MR, Faria MGI, Linde GA, Rubira AF, Muniz EC, Recent Advances in Designing Hydrogels from Chitin and Chitin-Derivatives and their Impact on Environment and Agriculture: A Review. *Revista Virtual de Química*. 2017; **9**: 1: 370–386. http://dx.doi.org.lproxy.yeditepe.edu.tr/10.21577/1984-6835.20170021 .
Crossref | CAS | Web of Science® | Google Scholar

73 Htwe Y, Chow W, Suda Y and Mariatti M, Effect of silver nitrate concentration on the production of silver nanoparticles by green method. *Mater Today* **17**: 568– 573 (2019).
Crossref | CAS | Google Scholar

74 Dayakar T, Rao KV, Park J, Sadasivuni KK and Rao KR, Non-enzymatic biosensing of glucose based on silver nanoparticles synthesized from *Ocimum tenuiflorum* leaf extract and silver nitrate. *Mater Chem Phys* **216**: 502– 507 (2018).
Crossref | CAS | Web of Science® | Google Scholar

75 Ravichandran V, Vasanthi S, Shalini S, Shah SAA, Tripathy M and Paliwal N, Green synthesis, characterization, antibacterial, antioxidant and photocatalytic activity of *Parkia speciosa* leaves extract mediated silver nanoparticles. *Results Phys* **15**: 102565 (2019).
Crossref | Web of Science® | Google Scholar

76 Aleksandrova G, Lesnichaya M, Dolmaa G, Klimenkov I, Sukhov B, Regdel D *et al*., Silver-containing nanocomposites with antioxidant activity based on humic substances of different origin. *Russ Chem Bull* **66**: 143– 149 (2017).
Crossref | CAS | Web of Science® | Google Scholar

77 Cáceres-Vélez PR, Fascineli ML, Sousa MH, Grisolia CK, Yate L, de Souza PEN *et al*., Humic acid attenuation of silver nanoparticle toxicity by ion complexation and the formation of a Ag^{3+} coating. *J Hazard Mater* **353**: 173– 181 (2018).
Crossref | CAS | PubMed | Web of Science® | Google Scholar

78 Khutsishvili SS, Lesnichaya MV, Vakul'skaya TI, Dolmaa G, Aleksandrova GP, Rakevich AL *et al*., Humic-based bionanocomposites containing stable paramagnetic gold nanoparticles for prospective use in pharmaceuticals. *Spectrosc Lett* **51**: 169– 173 (2018).
Crossref | CAS | Web of Science® | Google Scholar

79 Khutsishvili SS, Vakul'skaya TI, Aleksandrova GP and Sukhov BG, Stabilized silver nanoparticles and nanoclusters Ag_n in humic-based bioactive nanocomposites. *J Clust Sci* **28**: 3067– 3074 (2017).
Crossref | CAS | Web of Science® | Google Scholar

80 Al-Dhabi NA, Mohammed Ghilan A-K and Arasu MV, Characterization of silver nanomaterials derived from marine *Streptomyces* sp. al-dhabi-87 and its in vitro application against multidrug resistant and extended-spectrum beta-lactamase clinical pathogens. *Nanomaterials* **8**: 279 (2018).
Crossref | Web of Science® | Google Scholar

81 Öztürk BY, Gürsu BY and Dağ İ, Antibiofilm and antimicrobial activities of green synthesized silver nanoparticles using marine red algae *Gelidium corneum*. *Process Biochem* **89**: 208– 219 (2020).
Crossref | Web of Science® | Google Scholar

82 Valsalam S, Agastian P, Arasu MV, Al-Dhabi NA, Ghilan A-KM, Kaviyarasu K *et al*., Rapid biosynthesis and characterization of silver nanoparticles from the leaf extract of *Tropaeolum majus*

L. and its enhanced in-vitro antibacterial, antifungal, antioxidant and anticancer properties. *J Photochem Photobiol B Biol* **191**: 65– 74 (2019).
Crossref | CAS | PubMed | Web of Science® | Google Scholar

83 Ghosh M, Mandal S, Roy A, Chakrabarty S, Chakrabarti G and Pradhan SK, Enhanced antifungal activity of fluconazole conjugated with Cu-Ag-ZnO nanocomposite. *Mater Sci Eng C* **106**: 110160 (2020).
Crossref | CAS | PubMed | Web of Science® | Google Scholar

Citing Literature

Download PDF